Chloride penetration in concrete under varying humidity and temperature changes
A numerical study

Tong, Liang yu; Šavija, Branko; Zhang, Mingzhong; Xiong, Qing Xiang; Liu, Qing feng

DOI
10.1016/j.conbuildmat.2024.138380

Publication date
2025

Document Version
Final published version

Published in
Construction and Building Materials

Construction and Building Materials 458 (2025) 138380

Contents lists available at ScienceDirect

Construction and Building Materials

journal homepage: www.elsevier.com/locate/conbuildmat

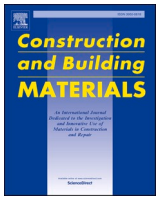

Chloride penetration in concrete under varying humidity and temperature changes: A numerical study

Liang-yu Tong [a], Branko Šavija [c], Mingzhong Zhang [d], Qing Xiang Xiong [a,e], Qing-feng Liu [a,b,e,*]

[a] State Key Laboratory of Ocean Engineering, School of Ocean and Civil Engineering, Shanghai Jiao Tong University, Shanghai, China
[b] State Key Laboratory of Subtropical Building and Urban Science, South China University of Technology, Guangzhou, China
[c] Microlab, Faculty of Civil Engineering and Geosciences, Delft University of Technology, Delft 2628CN, the Netherlands
[d] Department of Civil, Environmental and Geomatic Engineering, University College London, London WC1E 6BT, UK
[e] Shanghai Key Laboratory for Digital Maintenance of Buildings and Infrastructure, Shanghai, China

ARTICLE INFO

Keywords:
Concrete
Chloride penetration
Wetting-drying
Temperature
Cyclic boundary

ABSTRACT

When serving in the marine environment, reinforced concrete structures are prone to be attacked by chloride ingress, which generally co-occurs with varying humidity and temperature changes. Therefore, considering the interaction between moisture transport and heat transfer, and their individual and coupling effects on chloride transport, this paper presents a novel numerical modelling framework for chloride penetration in concrete under different environmental conditions. In this framework, a novel thermal conductivity model and temperature-depended chloride binding isotherms are also developed, considering the heterogeneous characteristics of concrete. The proposed model is validated against a series of experimental data. By assuming the cyclic humidity and temperature boundary conditions as trigonometric type, this study further discusses the effect of average value, amplitude value and period length of cyclic environmental changes on the chloride transport in concrete. The results indicate that variation in humidity and temperature averages can alter the peak values of chloride content but have less effect on the chloride penetration depth. However, the increased humidity amplitude could significantly promote both the peaks and the penetration depths due to intensive chloride convection caused by moisture transport. This paper is supposed to provide a better understanding of chloride penetration in concrete under a realistic engineering environment.

1. Introduction

The chloride-induced corrosion problem is recognised as one of the most deleterious factors causing durability degradation of reinforced concrete (RC) structures served in marine or offshore regions. The concentration gradient of chloride between the seawater and the internal pore solution of concrete will lead to the chloride diffusion in concrete cover and finally result in the structure damage, e.g., the corrosion of embedded rebars, which plays a vital role in the service life prediction and durability assessment of concrete structures [1,2]. Besides, due to the diurnal temperature differences or seasonal variations and dry-wetting cycles, concrete structures are always exposed to chloride ingress under varying temperatures and humidities conditions [3,4]. Thus, in this condition, the effect of temperature and humidity changes on chloride penetration should not be ignored, and the investigation of chloride ingress subjected to an unsaturated non-isothermal state is of great significance for both structure design and maintenance [5–9].

In the past decades, the ingress process of chloride in concrete structures under isothermal and saturated conditions has been widely studied both experimentally and numerically [10–14]. However, with the temperature and humidity changes, chloride penetration will be affected by the moisture and heat transfer and become more complex, and has rarely been investigated [15–18]. In the past few years, some studies have considered the effect of temperature on the rates of chloride and moisture transport during wetting-drying cycles [15,19–22]. However, in their studies, the environmental temperature was kept constant for simulations, and the coupling interaction between moisture and heat transfer was not considered. In recent years, a series of experimental and analytical studies on the interaction between any two of chloride, moisture and heat transport have been conducted in Refs. [6,23–26], but

* Corresponding author at: State Key Laboratory of Ocean Engineering, School of Ocean and Civil Engineering, Shanghai Jiao Tong University, Shanghai, China.
E-mail address: liuqf@sjtu.edu.cn (Q.-f. Liu).

https://doi.org/10.1016/j.conbuildmat.2024.138380
Received 20 April 2024; Received in revised form 13 September 2024; Accepted 15 September 2024
Available online 16 December 2024

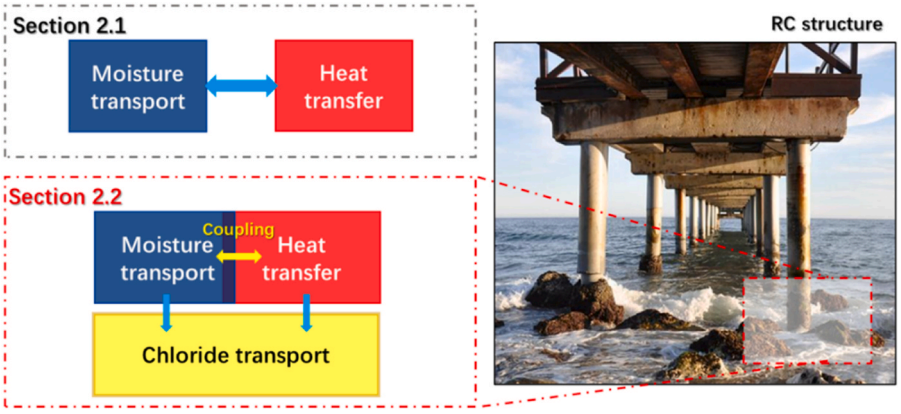

Fig. 1 Illustration of individual and coupled transport processes.

the coupled chloride-moisture-heat transport was not addressed. Additionally, although it has been widely accepted that the rising temperature can promote both moisture and chloride transport [8,23,27,28], the interaction between moisture transport and heat transfer has rarely been studied. Unsaturated concrete can be regarded as a composite consisting of a solid skeleton and water- and gas-filled pore structures with different thermal conductivities [29–31]. Therefore, the moisture transport can change the water content and distribution, affecting the ions' transport channels and the concrete's thermal conductivity. The heat transfer, in turn, would influence the moisture transport process. Therefore, more research is required to explore coupled moisture and heat transfer processes and analyse their coupling effect on chloride transport under varying humidity and temperature changes.

It is difficult, if not impossible, to experimentally consider different phenomena during coupled chloride-moisture-heat transport in concrete structures. Therefore, numerical studies would offer effective tools for estimating the effects of various parameters on such complex phenomena [23,32–34]. Because chloride ions may adhere to the cement matric of the pore structure physically and chemically [35], which decelerates the chloride transport, the effect of chloride binding must be considered for chloride transport modelling. At present, it has been reported experimentally that chloride binding capacity would be altered at different temperatures [36,37]. However, how to consider the different chloride binding capacities at varied temperatures in chloride transport modelling still needs further research. Moreover, realistic engineering environments are always diverse, where the temperature, relative humidity, and surface chloride concentrations often experience cyclical variations [38–41]. Although some existing numerical models were developed to analyse the chloride transport process subjected to wetting-drying cycles, the temperature variation was always ignored. To the best of the author's knowledge, the numerical study on chloride transport in cementitious materials accounting for both cyclically varied humidity and temperature boundary conditions is still lacking.

In this study, a numerical model was proposed to investigate chloride transport under varying humidity and temperature changes. Transport properties of concrete, including chloride diffusion coefficient, moisture diffusion coefficient and thermal conductivity, are determined based on the heterogeneous characteristics of concrete, which are related to changed humidity and temperatures. The intrinsic interaction of moisture transport and heat transfer, as well as their individual and coupling effects on the chloride ingress, are comprehensively analysed and discussed. The chloride distributions, including free and bound chlorides, in cementitious materials under various environmental conditions are predicted and validated with experimental data from the literature. In addition, the effects of the average value, amplitude value and period length of cyclic environmental humidity and temperature changes on the chloride transport process in concrete are discussed quantitatively.

2. Model setup

To model the coupled processes of chloride transport, moisture and heat transfer, two procedures will be carried out in this section, as shown in Fig. 1. Firstly, coupled moisture and heat transfer, as well as their interaction relationship, will be analysed in Section 2.1. Then, considering the individual effect of moisture and heat transfer and their coupled effect on chloride penetration, the chloride transport process under varying humidity and temperature changes will be modelled in Section 2.2.

2.1. Coupled moisture and heat transfer

2.1.1. Governing equation

Moisture serves as the transport medium for chloride ions. In unsaturated concrete, moisture transport in both gaseous and liquid water states, which are driven by the vapour pressure difference and capillary pressure differences, respectively. The moisture flux J is proportional to the gradient of pore pressure or pore relative humidity, as:

$$J = -(K_l \nabla P_c + K_v \nabla P_v) = -\left(K_l \frac{\partial P_c}{\partial h} + K_v \frac{\partial P_v}{\partial h}\right) \nabla h \# \quad (1)$$

Where h is the relative humidity, P_c is the capillary pressure of liquid water, P_v is the vapor pressure. Parameters K_l and K_v refer to the permeability of the liquid and vapour, respectively. Thus, the mass balance equation can be derived as follows [15,42,43]:

$$\frac{\partial S}{\partial t} = \frac{\partial h}{\partial t}\frac{\partial S}{\partial h} = -\nabla J = \nabla\left(K_l \frac{\partial P_c}{\partial h} + K_v \frac{\partial P_v}{\partial h}\right) \nabla h \quad (2)$$

where S is saturation degree. Then, the transport of moisture can be described by introducing moisture diffusion coefficient, as [19,44]:

$$\frac{\partial h}{\partial t} = \nabla(D_l + D_v)\frac{\partial h}{\partial S}\nabla h = \nabla D_h \nabla h \quad (3)$$

where D_h, D_l and D_v refer to moisture, liquid phase and vapour phase diffusion coefficient, respectively (m^2/s). $\partial S/\partial h$ is the moisture capacity which represents the slope of water sorption isotherms. For the water wetting process, a relationship between water saturation (S_w) and relative humidity can be written as [45,46]:

$$S_w = 1 - \exp\left[\frac{m_{w/c} - 1}{1.4 \ln\left(\frac{1}{h}\right)}\right] \quad (4)$$

where $m_{w/c}$ is the water to cement ratio. During the drying process, the water isotherm curve is always higher than the corresponding wetting

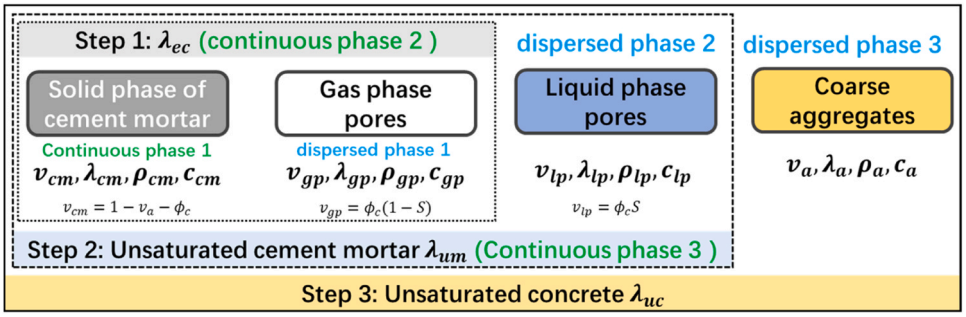

Fig. 2 Steps to calculate the thermal conductivity of unsaturated concrete.

curve because that water can be trapped in larger pores when connected to smaller pores [24,47]. Thus, the relationship between water saturation (S_d) and relative humidity during the drying process can be described as [48]:

$$S_d = S_w + S_{trap} = S_w(1 - \ln S_w) \tag{5}$$

Considering the moisture capacities for drying and wetting processes are different, the moisture diffusion coefficients should be assigned to the drying and wetting processes respectively as follows [15,49]:

$$D_h = \begin{cases} D_d^0\left[\alpha + \dfrac{1-\alpha}{1+\left(\frac{1-h}{1-h_c}\right)^{n_1}}\right] & \text{drying} \\ D_w^0 \exp(n_2 h) & \text{wetting} \end{cases} \tag{6}$$

where D_d^0 and D_w^0 are the moisture diffusion coefficient of concrete at dry and saturated state, respectively, α is the ratio of minimum D_h to D_d^0, h_c is the relative humidity when $D_h = D_d^0/2$, n_1 and n_2 refer to the parameters that characterise the spread of drop and rise in moisture diffusion coefficients. Here, $\alpha = 0.025$, $h_c = 0.8$, $n_1 = n_2 = 6$ are assumed according to the [49]. Considering moisture and heat transfer are coupled together in the present study, **Eq. (6)** should be modified by taking into account the influenced of temperature, as [23,50]:

$$D_h = \begin{cases} D_d^0\left[\alpha + \dfrac{1-\alpha}{1+\left(\frac{1-h}{1-h_c}\right)^{n_1}}\right] \exp\left[\dfrac{U}{R}\left(\dfrac{1}{T_{ref}} - \dfrac{1}{T}\right)\right] & \text{drying} \\ D_w^0 \exp(n_2 h) \exp\left[\dfrac{U}{R}\left(\dfrac{1}{T_{ref}} - \dfrac{1}{T}\right)\right] & \text{wetting} \end{cases} \tag{7}$$

where U is the activation energy of the diffusion process (35000 J • mol), R is the gas constant (8.14 J • mol^{-1} • K^{-1}), T is the temperature (K) and T_{ref} is the reference temperature (296 K).

The governing equation of heat transfer in unsaturated concrete, excluding convection phenomena, can be expressed as [51,52]:

$$\rho c(S)\frac{\partial T}{\partial t} = \nabla\frac{\lambda_c(S)}{C_c(S)}\nabla T \tag{8}$$

where λ_c and C_c are thermal conductivity (W/m/K) and thermal capacity (J/m^3/K) of concrete, respectively and C_c equals to the product of specific heat capacity (c, J/kg/K) and density (ρ, kg/m^3) of the material. It is important to note that the heat released and absorbed during the condensation and evaporation of moisture is not considered in the present study, as the focus is on the overall moisture diffusion process. Considering the effect of moisture transport on heat transfer, unsaturated concrete should be regarded as a multi-phase-composite consisting of solid, liquid and gaseous phases, which own different thermal conductivities, specific capacities and densities [53]. To determine the thermal conductivity of unsaturated concrete, an analytical model will be introduced next.

2.1.2. *Thermal conductivity model of unsaturated concrete*

Due to the heterogeneous nature of concrete [54], different components of concrete correspond to different thermal conductivities [55]. Therefore, this section will take several steps to calculate the thermal conductivity of unsaturated concrete, as shown in Fig. 2.

Firstly, at step 1, by treating gas phase pores as the dispersed phase, the effective thermal conductivity of cement mortar with gas phases can be obtained by Maxwell's model, which is a kind of theoretical model to calculate the effective thermal conductivity of two-phase composite, as follows [51,56]:

$$\lambda_{ec} = \lambda_{cm}\frac{2\lambda_{cm} + \lambda_{gp} - 2(\lambda_{cm} - \lambda_{gp})\dfrac{v_{gp}}{v_{gp} + v_{cm}}}{2\lambda_{cm} + \lambda_{gp} + (\lambda_{cm} - \lambda_{gp})\dfrac{v_{gp}}{v_{gp} + v_{cm}}} \tag{9}$$

where λ_{ec}, λ_{cm} and λ_{gp} are the effective thermal conductivity of cement mortar with gas phases, solid phase of cement mortar and gas phase pores, respectively. v_{gp} and v_{cm} are volume fraction of gas phase pores and solid phase of cement mortar.

Then, at step 2, unsaturated cement mortar can be considered to be a two-phase composite, which regards liquid phase pores (dispersed phase) are randomly dispersed within cement mortar with gas phase pores (continuous phase, which thermal conductivity has been calculated at step 1). Similarly, the effective thermal conductivity of unsaturated cement mortar can be obtained by Maxwell's model as [57]:

$$\lambda_{um} = \lambda_{ec}\frac{2\lambda_{ec} + \lambda_{lp} - 2(\lambda_{ec} - \lambda_{lp})\dfrac{v_{lp}}{v_{gp} + v_{cm} + v_{lp}}}{2\lambda_{ec} + \lambda_{lp} + (\lambda_{ec} - \lambda_{lp})\dfrac{v_{lp}}{v_{gp} + v_{cm} + v_{lp}}} \tag{10}$$

where λ_{um} and λ_{lp} are the effective thermal conductivity of unsaturated mortar and liquid phase pores, respectively. v_{lp} is the volume fraction of liquid phase pores in concrete, $v_{lp} = S\phi_c$; ϕ_c is the porosity of concrete.

Finally, at step 3, assuming that coarse aggregates (dispersed phase) are randomly dispersed in the unsaturated cement mortar (continuous phase). The effective thermal conductivity of unsaturated concrete can also be calculated still by adopting Maxwell's model as:

$$\lambda_{uc} = \lambda_{um}\frac{2\lambda_{um} + \lambda_a - 2(\lambda_{um} - \lambda_a)v_a}{2\lambda_{um} + \lambda_a + (\lambda_{um} - \lambda_a)v_a} \tag{11}$$

where λ_{uc} and λ_{lp} are the effective thermal conductivity of unsaturated concrete and coarse aggregates, respectively. However, the Interfacial Transition Zone (ITZ) weakens the bond between aggregate and cement paste due to its higher porosity and microcracking tendencies, impacting the overall strength and durability of concrete [58,59]. It was also reported that interfacial resistance would occur between cement mortar

Table
1Physical characteristics of solid, liquid and gaseous phases at 293 K [51,53,56].

Component	λ (W/m/K)	ρ (kg/m^3)	c (J/kg/K)
Cement mortar	1.78	2941.4	920
Gas phase pores	0.0267	1.225	1006.43
Water phase pores	0.58	998.2	4182
Coarse aggregates	2.55	2733	820

and coarse aggregate, and affect the heat transfer. In this case, the effective thermal conductivity of unsaturated concrete should be determined considering interfacial resistance by using Hasselman--Johnson's model [60]:

$$\lambda_{uc} = \lambda_{um}\frac{2\lambda_{um} + \lambda_a(1+\beta) - 2[\lambda_{um} - \lambda_a(1-\beta)]v_a}{2\lambda_{um} + \lambda_a(1+\beta) + [\lambda_{um} - \lambda_a(1-\beta)]v_a} \tag{12}$$

where β is the interfacial thermal resistance coefficient, depending on the saturation degree of concrete, as [56]:

$$\beta = 0.6369 \bullet S^3 - 1.0338 \bullet S^2 + 0.1728 \bullet S + 0.2235 \tag{13}$$

In unsaturated concrete, thermal conductivity can also be calculated based on the volume proportions of solid, liquid and gas phases, as [50]:

$$C_c(S) = (1 - \varnothing_c - v_a)\rho_{cm}c_{cm} + \varnothing_c S\rho_{lp}c_{lp} + \varnothing_c(1-S)\rho_{gp}c_{gp} + v_a\rho_a c_a \tag{14}$$

where c_{cm} ρ_{cm}, c_{lp} ρ_{lp}, c_{gp} ρ_{gp} and c_a ρ_a are the specific heat capacity and density of cement mortar, liquid phases, gaseous phases and coarse aggregates, respectively. In the present study, the parameters entered to calculate the thermal conductivity of unsaturated concrete are listed in Table 1. It is important to note that the heat capacities and densities of different phases will also change with temperature. However, given that the change is small, it is ignored in the present thermal conductivity model [53]. The validation of the proposed thermal conductivity model and the coupled moisture and heat transfer model will be carried out in Section 3.1.

2.2. Chloride transport under varying humidity and temperature changes

2.2.1. Governing equation

Chloride transport in concrete can be regarded as coupling servals basic transport mechanisms, such as diffusion, migration, adsorption and pressure-induced flow [32,61,62]. In unsaturated concrete with no applied electric field, chloride transport mainly depends on chloride diffusion caused by the ionic concentration gradient and chloride convection caused by moisture transport [6,63]. The flux of chloride ions J_{cl} in an unsaturated concrete can be expressed as [64,65]:

$$J_{cl} = J_{diff} + J_{conv} = -D_{cl}(S)\nabla C_{cl} - D_h C_{cl}\nabla h \tag{15}$$

where J_{diff} and J_{conv} are the chloride flux related to chloride diffusion and chloride convection (mol/m^2/s), respectively, C_{cl} is the total chloride concentration (mol/m^3), $D_{cl}(S)$ is the chloride diffusion coefficient (m^2/s), which is strongly related to water saturation. In the present study, $D_{cl}(S)$ is assumed as $D_c \bullet S^r$, in which D_c is the chloride diffusion coefficient of saturated concrete and $r = 1$ is parameter [66,67]. Some empirical or theoretical equations have been developed to determine the chloride diffusivity of saturated cement paste. This work adopts the equation proposed by Zheng and Zhou [68] which is derived based on the generalized effective medium theory, as:

$$D_{cp} = \frac{2\phi_{cp}^{2.75}D_0}{\phi_{cp}^{1.75}(1-\phi_{cp}) + 14.44(1-\phi_{cp})^{2.75}} \tag{16}$$

where D_{cp} is the chloride diffusion coefficient of saturated cement paste, D_0 represents the chloride diffusion coefficient in pore solution (2.03×10^{-9}), $\varnothing_{cp}$ is the porosity of the cement paste. However, in concrete, the presence of aggregates will increase the effective length travel by a flux. Therefore, by adopting Cidiac and Shafikhani formulation for tortuosity factor (f_τ), the chloride diffusion coefficient of concrete should be modified as [69]:

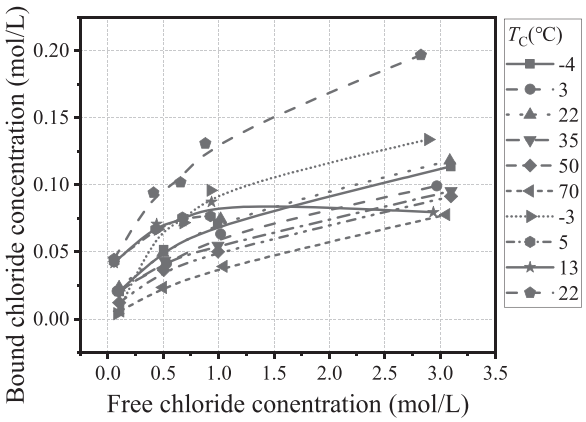

Fig. 3 Measured bound chloride concentration exposed to different temperatures.

$$D_c = D_{cp}f_\tau = D_{cp}\frac{3(1-v_a)^2}{3-v_a} \tag{17}$$

Moreover, during chloride transport, some ions react with hydration products to produce Friedel's salt, and some are adsorbed on the surface of hydrated calcium silicate or closed between the layers of C-S-H, which decelerates the chloride transport. Therefore, the effect of chloride binding must be considered during the chloride transport modelling [36,70]. The relationship between total, bound (C_b) and free (C_f) chloride concentration can be expressed as [34,71,72]:

$$C_{cl} = C_b + SC_f \tag{18}$$

Appling **Eq. (15, 18)** into mass conversation equation and considering only free chloride can transport, the governing equation of chloride transport can be written as:

$$\frac{\partial C_{cl}}{\partial t} = (\frac{\partial C_b}{\partial C_f} + S)\frac{\partial C_f}{\partial t} = \nabla\left(D_c S\nabla C_f + D_h C_f \nabla h\right) \tag{19}$$

By defining $\frac{\partial C_b}{\partial C_f}$ as γ, it yields:

$$\frac{\partial C_f}{\partial t} = \nabla\frac{1}{S+\gamma}\left(D_c S\nabla C_f + D_h C_f\nabla h\right) \tag{20}$$

Under varying humidity and temperature changes, the movement of chloride ions and the amount of bound chloride ions can be affected by temperature. Therefore, at different temperatures, **Eq. (20)** should be modified by taking into account the influence of temperature as [52,73,74]:

$$\frac{\partial C_f}{\partial t} = \nabla\frac{1}{S+\gamma(T)}\left(D_0 S f_T(T)\nabla C_f + D_h C_f f_T(T)\nabla h\right) \tag{21}$$

$$f_T(T) = \exp\left[\frac{U}{R}\left(\frac{1}{T_{ref}} - \frac{1}{T}\right)\right] \tag{22}$$

The relationship between bound and free chloride concentration at changed temperatures is still challenging to determine directly. Thus, the present study will propose an empirical binding isotherm by fitting experimental data, as illustrated in the next section.

2.2.2. temperature-dependent chloride binding isotherm

For Ordinary Portland Cement (OPC)-based materials, to describe the chloride binding capacity, the linear, Langmuir and Freundlich binding isotherms are often described as follows [12,75]:

Table
2Fitted binding parameters by using Langmuir and Freundlich isotherms.

T	Langmuir			Freundlich			Ref.
	$A(10^{-1})$	$B(10^{-1})$	R^2	$A(10^{-2})$	$B(10^{-1})$	R^2	
−4	1.54	10.45	0.9820	6.87	4.57	0.9917	[76]
3	1.23	9.81	0.9416	6.02	4.62	0.9907	
22	1.53	9.76	0.9694	7.02	4.63	0.9966	
35	1.22	9.84	0.9333	5.68	4.54	0.9969	
50	0.897	6.69	0.9855	4.99	5.39	0.9957	
70	0.522	3.47	0.9985	3.67	6.75	0.9958	
−3	2.05	11.69	0.9639	8.56	4.71	0.9099	[37]
5	15.9	200.3	0.9550	7.99	2.14	0.9880	
13	1.44	17.3	0.8810	8.55	2.53	0.9866	
22	3.37	13.9	0.8971	13.1	3.91	0.9897	

$$C_b = \mathrm{A}C_f \tag{23}$$

$$C_b = \frac{\mathrm{A}C_f}{1 + BC_f} \tag{24}$$

$$C_b = \mathrm{A}C_f^B \tag{25}$$

where A and B are binding parameters.

Here, the measured bound chloride concentration under different temperatures and different free chloride concentrations by Dousti and Shekarchi [76], and Panesar et al. [37] are collected, as shown in Fig. 3. In Dousti and Shekarchi's work, ASTM Type II OPC was used, with $m_{w/c}$ of 0.4. NaCl solution of four initial concentrations, 0.1, 0.5, 1 and 3 mol/L were tested. In Panesar et al.'s work, Type I OPC with $m_{w/c}$ of 0.3 was adopted, and NaCl solution of five initial concentrations, 0.1, 0.5, 0.75, 1, and 3 mol/L were used.

It can be seen from Fig. 3 that the linear binding isotherm was too simple to describe the non-linear binding capacity accurately. Therefore, Langmuir and Freundlich isotherms are used in this section to fit the measured data. Table 2 summarises the fitted binding parameters (A and B) at different temperature. It can be seen that Freundlich isotherm provides a better fitting accuracy. To obtain a general relationship that describes the influence of temperature on chloride binding, the parameters A and B are considered temperature-dependent and expressed as a polynomial function of temperature, as follows:

$$A = a_1 T_C^2 + b_1 T_C + c_1 \tag{26}$$

$$B = a_2 T_C^2 + b_2 T_C + c_2 \tag{27}$$

Fig. 4 shows the parameters A and B against exposure temperature for all samples. T_C denotes temperature in degree Celsius. The fitted equations are also shown in the figures. The fitted results indicate a non-linear relationship between temperature and the chloride binding capacity. This may relate to the fact that while increased temperature can enhance the chemical binding due to an increased reaction rate, the physical binding of chloride will be hindered due to the higher thermal vibration of chloride ions [76]. In Section 3.2, the coupled chloride transport, moisture, and heat transfer model will be validated by comparing it with a series of experimental data, including non-isothermal chloride transport, chloride transport subjected to drying-wetting cycles and chloride transport under varying humidity and temperature changes.

3. Model validation

To validate the proposed model of chloride transport in concrete structures under varying humidity and temperature changes, this section will compare the modelled results with a series of published experimental data. Corresponding to the model setup illustrated in Section 2, the validation will be done through two sections. Firstly, the thermal conductivity model and coupled moisture and heat transfer model will be validated in Section 3.1. Then, the modelling of chloride transport under different environmental conditions will be validated in Section 3.2. Since the lateral surfaces of the specimens in the adopted experiments were sealed, the transport processes in concrete can be considered one-dimensional and, therefore, will be modelled in one dimension in this section. Details of experiments will be illustrated in the later sections. The effect of aggregates on chloride transport, moisture and heat transfer process are considered through transport parameters. Parameters used in the proposed model are concluded in Appendix Table A.

3.1. Coupled moisture and heat transfer

3.1.1. Thermal conductivity

To validate the proposed thermal conductivity model, the predicted thermal conductivities of OPC-based concrete with different volume fractions of aggregates, saturation degrees and $m_{w/c}$ are compared with experimentally measured results from Zhang et al.'s work [56]. In the experiment, OPC with a density of 3097 kg/m^3 was used. Crushed limestone and natural river sand were used as coarse and fine aggregates, with densities of 2733 kg/m^3 and 2639 kg/m^3, respectively. Thermal conductivities of dry concrete were measured by means of guarded hot plate apparatus [77], while thermal conductivities of unsaturated concrete were measured by means of a transient plane source [78]. Specimens with different volume fractions of aggregates, saturation degree and $m_{w/c}$ were all sized at 250 × 250 × 50mm. Before

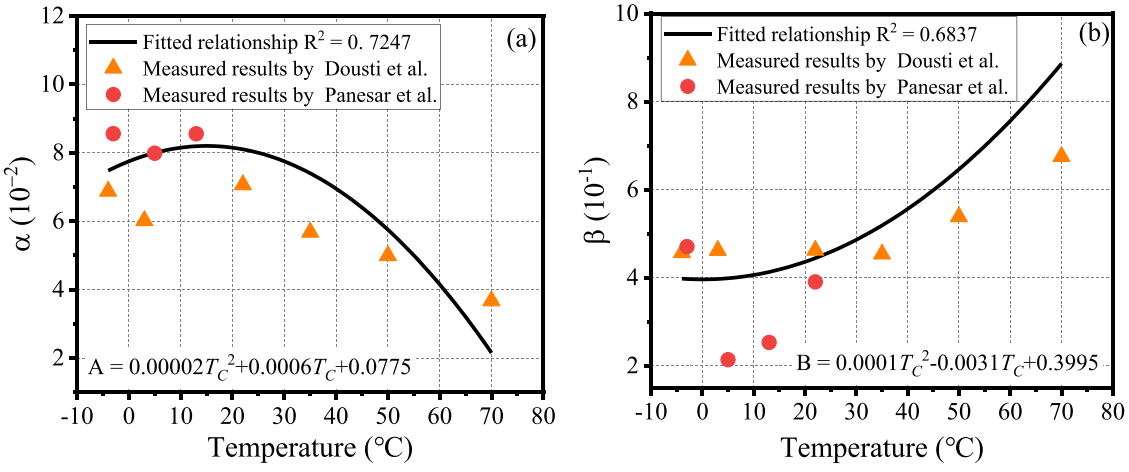

Fig. 4 Relationship between temperature and binding parameters (a) A, (b) B.

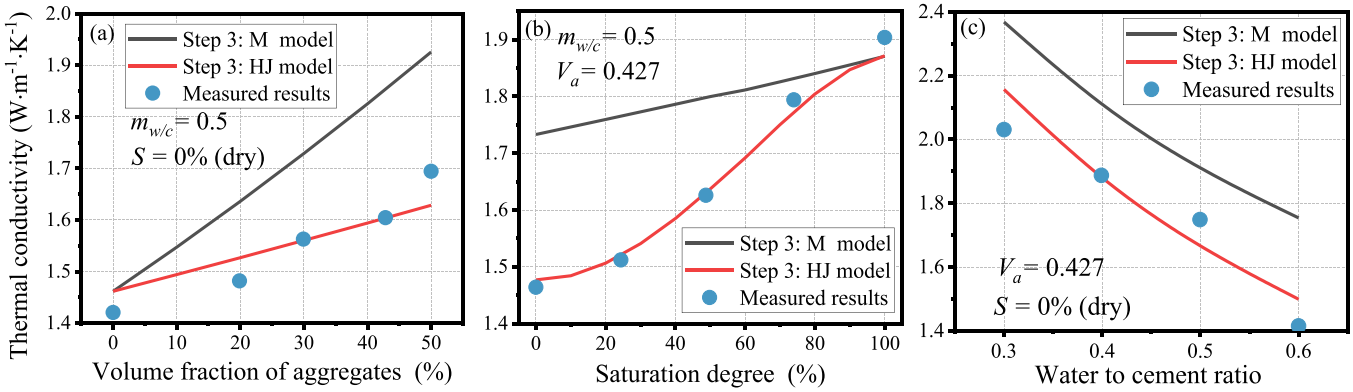

Fig. 5 Comparison of modelled and measured thermal conductivities of concrete with (a) different volume fractions of aggregates, (b) saturation degree and (c) water to cement ratio. Notice: M presents using Maxell's model in the 3rd step of the model; HJ presents using Hasselman-Johnson's model.

Table
3Boundary and initial conditions of different field variables in concrete [79].

Field variables	Initial conditions		Boundary conditions	
	h_0	T_0(K)	h_s	T_s(K)
Condition 1	50 %	293	100 %	313
Condition 2	50 %	293	100 %	333

Notice: h_0 and T_0 are the initial relative humidity and temperature, respectively. h_s and T_s are the boundary relative humidity and temperature, respectively.

measuring thermal conductivity, all specimens were kept in a saturated curing room at 20 ± 2℃ and 95 % relative humidity for 28 days. Based on the mix proportions, the comparison of modelled and measured results of thermal conductivities is shown in Fig. 5.

The results indicate Maxell's model would overestimate the thermal conductivities of concrete due to the ignorance of interfacial resistance between cement mortar and coarse aggregate. On the contrary, the predicted thermal conductivities using Hasselman-Johnson's model in the 3rd step of the model can obtain reliable results. Because coarse aggregate has a greater conductivity than cement mortar, the thermal conductivity of concrete in a dry state will also increase with the increasing volume fraction of coarse aggregates, as shown in Fig. 5**(a)**. In the same way, due to the thermal conductivity of water being much higher than air, the thermal conductivity of concrete increases with the increasing saturation degree, as shown in Fig. 5**(b)**. In addition, considering that the porosity (air volume) of concrete increases with the increasing water to cement ratio, thus concrete in a dry state has a decreasing thermal conductivity trend with the increasing water to cement ratio, as shown in Fig. 5**(c)**.

3.1.2. Moisture and temperature variation

Experimental work done by Wang and Xi [79] is used in this section to validate the coupled moisture and heat transfer in concrete. In their experiment, Ordinary type I Portland cement was used. The samples were prepared with a water to cement ratio of 0.6 and a gravel to cement ratio of 2.9. After demoulding, cylindrical specimens (6 in. × 12inch) were cured at 20 °C and 100 % relative humidity for 28 days and then kept in the ambient environment to reach the initial conditions with 20 °C and 50 % relative humidity. In their experiments, the lateral surfaces and bottom side were sealed by several layers, including silicone, foam isolation and cable ties to avoid exchanges of heat and moisture with the environment. Only the top surface was placed in a container filled with distilled water and heated by an electric heater. The boundary and initial conditions are given in Table 3. The change of temperature and relative humidity inside the sample at the position 63.5 mm from the top was measured by the inserted sensors.

Fig. 6 compares the modelled and measured variation of relative humidity and temperature over time at different conditions. The modelled results with and without considering the interaction between moisture and heat transfer are also compared. As shown in Fig. 6 **(a-1)** and **(a-2)**, the moisture transport is significantly accelerated by the increased environmental temperature, and the influence is obvious at the beginning of the transport process. This is related to the rapid temperature growth in the first two days, as shown in Fig. 6 **(b-1)** and **(b-2)**. After three days, the temperature change is relatively small, and the impact on moisture transport is limited. If the interaction between moisture and heat transfer is ignored, which means that thermal conductivity remains constant at different saturation degrees and moisture diffusion coefficient does not change with temperature, the predicted relative humidity and temperature will be underestimated, as shown in Fig. 6. This is because that the elevated temperature can promote the moisture transport and the increased water saturation will also accelerate the heat transfer. The predicted results also indicate that considering the interaction relationship for modelling moisture and heat transfer processes is important.

3.2. Chloride transport under different environments

3.2.1. Under the non-isothermal condition

The chloride ingress tests done by Samson and Marchand [52] are used in this section to validate the modelled chloride transport process under non-isothermal conditions. In the experiment, the hydrated cement paste was prepared with an ordinary Canadian Type 10 Portland cement with water to cement ratio of 0.6. The lateral surface of the cylindrical specimens (diameter 10 cm, length 50 mm) was coated with silicon gel. The chloride immersion tests were conducted on saturated cement paste exposed to 0.5 mol/L NaCl solution. The initial temperature of 50-mm specimens was kept at 23 ℃, and the immersion test lasted 100 days at 4, 23 and 38 ℃, respectively. Fig. 7 compares modelled and measured chloride concentration distribution at different immersion temperatures.

The results show a good correlation between the modelled and measured results, and the increased temperature will promote the chloride transport process. The predicted chloride distribution by keeping the constant temperature of 23 ℃ will overestimate the chloride content at 4 ℃ and underestimate the chloride content at 38 ℃, demonstrating the importance of considering the effect of temperature during chloride transport modelling.

3.2.2. Subjected to drying-wetting cycles

This section will validate the modelling of coupled chloride and moisture transport processes while keeping the environmental temperature constant. The chloride transport process in cement mortars exposed to alternate drying-wetting cycles tested by Iqbal and Ishida

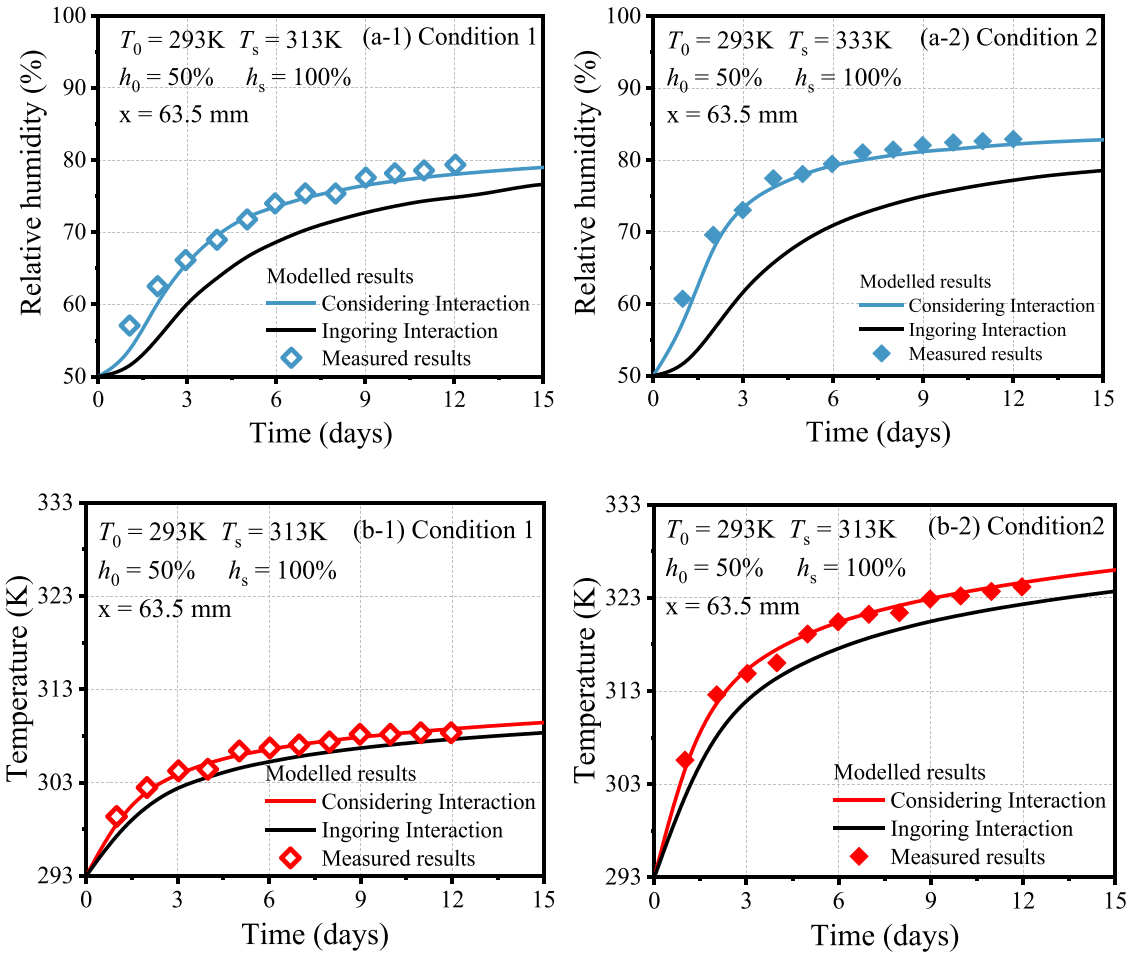

Fig. 6 Comparison of predicted and measured results after exposure to different environmental conditions (a-1) relative humidity variation in condition 1, (a-2) relative humidity variation in condition 2; (b-1) temperature variation in condition 1 (b-2) temperature variation in condition 2.

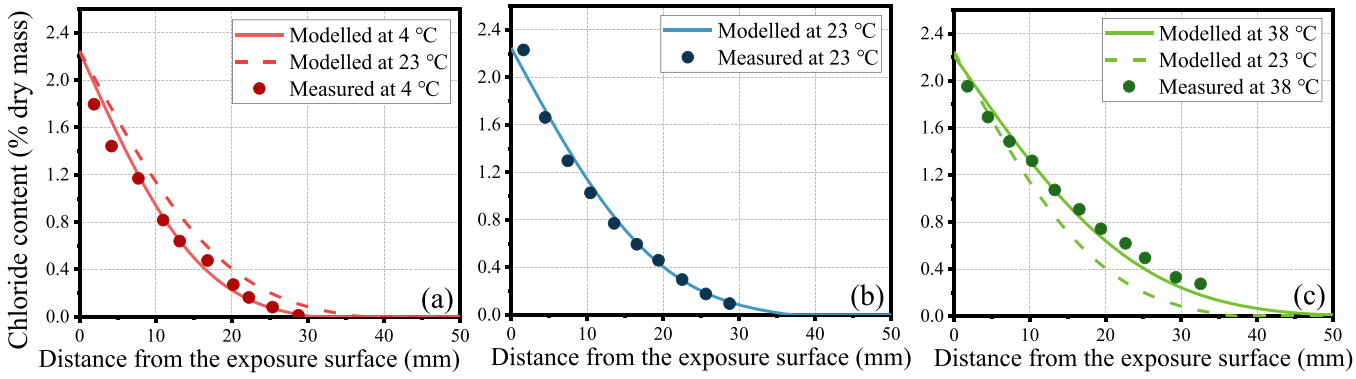

Fig. 7 Comparison of modelled and measured chloride content after 100 days exposure at temperature (a) 4 ℃, (b) 23 ℃ and (c) 38 ℃.

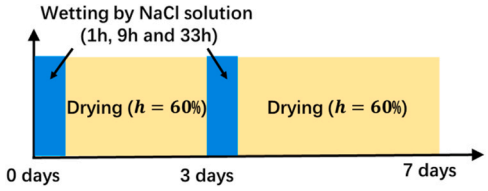

Fig. 8 Weekly exposure cycle for alternate wetting and drying experiment.

[67] is chosen to compare with modelled results. In the experiment, all specimens were prepared by OPC with water to cement ratio of 0.5 and sand to cement ratio of 2.25. Specimens consist of cylinders 50 mm in diameter and 100 mm in height. After curing at 20 °C for 28 days, all the specimens were sealed with one face exposed. Then, all the specimens were placed inside an environment control chamber with 60 % relative humidity and 20 °C temperature for 30 days before drying-wetting tests. As shown in Fig. 8, three wetting-to-drying exposure cycles (W/D) were designed weekly to represent the different tidal levels in the marine environment.

After exposing to 6% NaCl solution by mass for 1, 7 and 12 months,

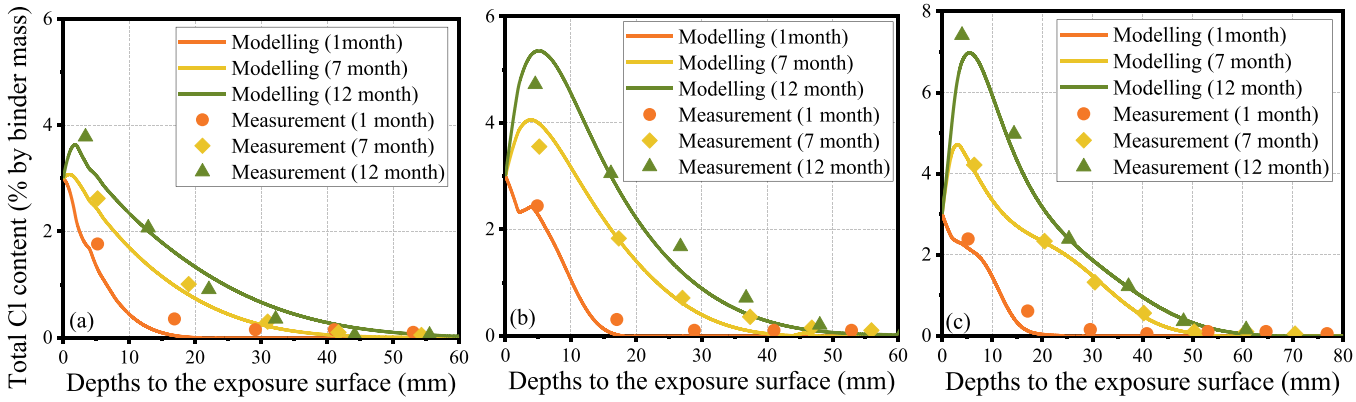

Fig. 9 Comparison of modelled and measured total chloride content during wetting-drying cycles for (a) 1 h wetting, (b) 9 h wetting, (c) 33 h wetting.

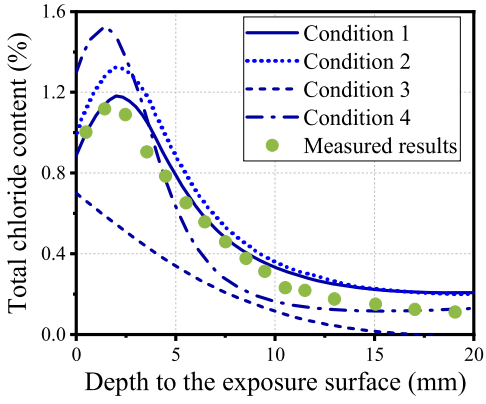

Fig. 10 Comparison of modelled and measured total chloride content under cyclic humidity and temperature changes.

the chloride concentration distribution was determined by the slicing method. For the wetting process, Dirichlet boundary conditions with C_{cl} = 6% by mass and h = 100 % are applied to chloride and moisture transport modelling, respectively. On the contrary, the Dirichlet boundary condition with h 60 % is applied to moisture transport for the drying process modelling, while the no-flux boundary condition should be used for chloride transport modelling. The comparison of modelled and measured chloride distribution is shown in Fig. 9, and good agreements between the two sets of data can be found. It is obvious that the more the number of W/D cycles, the deeper chlorides can penetrate. Due to the cyclic W/D processes, the convection process caused by moisture transport will lead to a significant accumulation of chloride content at the area close to the exposure surface for a long-term period. The chloride distribution profiles obtained by considering combined diffusion and convection processes in Fig. 9 are obviously different from those shown in Fig. 7, which indicates the importance of considering the effect of moisture transport on chloride penetration under varying relative humidity changes. It can also be found that the increasing wetting time will lead to higher peak values in the chloride contents. However, the penetration depth of chloride ions is generally constant regardless of different W/D conditions.

3.2.3. Under cyclic humidity and temperature changes

After validating the couple moisture-heat transfer in Section 3.1.2, couple heat-chloride transport in Section 3.2.1 and coupled moisture-chloride transport in Section 3.2.2, respectively, this section will validate the modelling of chloride transport under varying humidity and temperature changes. Herein, the experimental work done by Sun et al. [80] is used. In their research, concretes were prepared with OPC 42.5, water to cement ratio of 0.4, gravel to cement ratio of 3 and sand to cement ratio of 1.66. The sizes of concrete specimens were set as 100mm × 100mm × 100mm. After being demoulded at 24 h, the specimens were cured at 20 °C and 90 % relative humidity for 27 days. The surface of the specimens for the tests was sealed by epoxy except for one lateral surface. During wetting, specimens will be immersed in 3.5 % NaCl solution at 23 °C. Then, the specimens will be dried in an oven at 50 °C. The W/D ratio was set as 1:2.5, and each cycle lasted 3.5 days. The whole experiment lasted 140 days.

Table
4Different environmental conditions used in the model.

	Environmental conditions
Condition 1	Relative humidity and temperature change cyclically, with chloride binding
Condition 2	Relative humidity and temperature change cyclically, without chloride binding
Condition 3	Relative humidity remains constant at 100 %, and temperature changes cyclically
Condition 4	Relative humidity changes cyclically, temperature remains constant at an average of 42 °C

The comparison of modelled and measured results is shown in Fig. 10. To further demonstrate the significant influences of environmental variations on chloride penetration, the chloride distributions under assumed environmental conditions (as listed in Table 4) are also modelled here. It can be seen that the predicted chloride content, considering cyclical relative humidity and temperatures (condition 1), shows a good agreement with measured results. On the contrary, if chloride binding is ignored (condition 2), the chloride content will be overestimated. Besides, when ignoring the effect of moisture transport on chloride penetration (condition 3), the chloride content will be significantly underestimated due to the absence of the convection process. In addition, when temperature remains constant (condition 4), the chloride content will be overestimated in the area near the surface and underestimated in the region away from the surface. This is because the average temperature 42 °C in condition 3 will accelerate the convective process in the wetting process. Overall, from Sections 3.1 to 3.2, the series of comparisons on modelled and measured results well demonstrates the effectiveness of the proposed method in terms of modelling the chloride transport under varying humidity and temperature changes.

4. Discussion

Under marine or offshore environments, concrete structures are exposed to cyclic wetting-drying cycles due to tidal or water splash, and ambient temperature also shows cyclical changes throughout the day or over time. Therefore, to better study the cyclic environmental conditions on chloride transport, boundary conditions of moisture and heat transfer

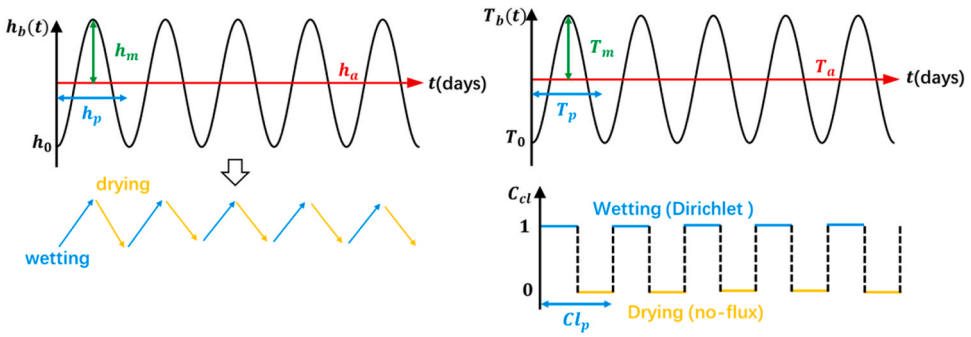

Fig. 11 Schematic description of the cyclic boundary condition of temperature, relative humidity and chloride concentration.

Table
5Input parameters of boundary humidity and temperature with changes in average values.

Condition	h_a	h_m	h_p	T_a	T_m	T_p	Results
h_a changes	50 % 60 % 70 % 80 %	20 %	10 (days)	298 K	10 K	10 (days)	Fig. 12 (a)
T_a changes	60 %	40 %	10 (days)	288 K 293 K 298 K 303 K	10 K	10 (days)	Fig. 12 (b)

are assumed as trigonometric function (**Eqs. (**28, 29**)**), with average h_a and T_a, amplitude h_m and T_m, as well as period h_p and T_p, accordingly.

$$h_s(t) = h_a + h_m \sin\left(2\pi \frac{t - h_p/4}{h_p}\right) \tag{28}$$

$$T_s(t) = T_a + T_m \sin\left(2\pi \frac{t - T_p/4}{T_p}\right) \tag{29}$$

As shown in Fig. 11, the initial humidity and temperature are set as minimum values. During repeated wetting and drying cycles, the boundary concentration of chloride transport would correspondingly change. Thus, the boundary period of chloride transport is assumed to coincide with the boundary period of moisture transport. During wetting, the boundary chloride concentration is set as 1 mol/m^3. The water to cement ratio and volume fraction of coarse aggregates of concrete are set as 0.5 % and 50 %, respectively. In this section, parametric analysis will be carried out to study the effect of average value, amplitude value and period length of cyclically changed boundary conditions on the chloride transport process.

4.1. *Effect of average value of $h_s(t)$ and $T_s(t)$ on chloride transport*

Keeping the amplitude value and period length of boundary conditions constant, the section compares chloride concentration profiles after 200 days of exposure at different average boundary humidity and temperature values. The detailed input parameters of $h_s(t)$ and $T_s(t)$ are listed in Table 5.

Fig. 12 shows the modelled total chloride concentration after 200 days. It can be found that increased average humidity or temperature would lead to higher chloride concentration and peak values. Besides, as shown in Fig. 12**(a)**, increased average humidity will not only promote the peak values but also the peak location of chloride distribution and penetration depths of chloride penetration slightly. This is because the higher average environmental humidity gives the concrete a higher saturation degree, which can accelerate the moisture and chloride transport. On the contrary, as shown in Fig. 12**(b)**, increased average temperature mainly affects the peak values of total chloride concentrations, while the peak locations and penetration depths remain generally constant. This also indicates that the chloride penetration depth is mainly dominated by moisture transport during the cyclic wetting-drying processes.

Table
6Input parameters of boundary humidity and temperature with changed amplitude values.

Condition	h_a	h_m	h_p	T_a	T_m	T_p	Results
h_m changes	60 %	10 % 20 % 30 % 40 %	10 (days)	298 K	10 K	10 (days)	Fig. 13 (a)
T_m changes	60 %	40 %	10 (days)	298 K	5 K 10 K 15 K 20 K	10 (days)	Fig. 13 (b)

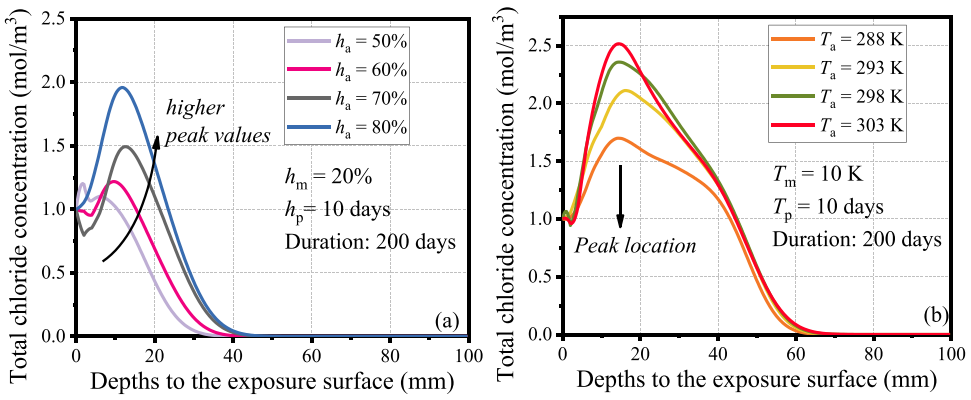

Fig. 12 Chloride concentration profiles at different average values of (a) $h_s(t)$ and (b) $T_s(t)$.

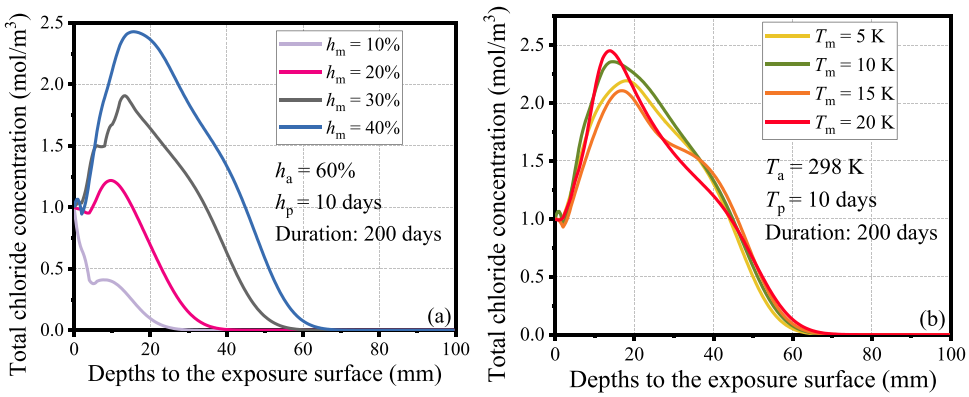

Fig. 13 Chloride concentration profiles at different amplitude values of (a) $h_s(t)$ and (b) $T_s(t)$.

Table
7Input parameters of boundary humidity and temperature with changed amplitude values.

Condition	h_a	h_m	h_p	T_a	T_m	T_p	Results
h_p changes	60 %	20 %	10 (days) 20 (days) 30 (days) 40 (days)	298 K	10 K	10 (days)	Fig. 14(a)
T_p changes	60 %	40 %	10 (days)	298 K	10 K	10 (days) 15 (days) 20 (days) 25 (days)	Fig. 14(b)

4.2. *Effect of amplitude value of* $\boldsymbol{h_s(t)}$ *and* $\boldsymbol{T_s(t)}$ *on chloride transport*

Similar to Section 4.1, this section remains the average value and period length of boundary conditions constant and compares chloride concentration profiles after 200 days of exposure at different amplitude values of boundary humidity and temperature. The detailed input parameters of $h_s(t)$ and $T_s(t)$ are listed in Table 6.

The predicted total chloride concentration profiles are shown in Fig. 13. It is apparent from Fig. 13**(a)** that as the humidity amplitude increases, there is a substantial increase in peak values, peak locations and the penetration depths of chloride ions. This is because an increase in boundary humidity amplitudes over the same period can lead to more intense chloride convection processes. This finding also agrees with Chen et al.'s experiments [81]. However, as shown in Fig. 13**(b)**, chloride distributions have less variability when the average temperature is held constant and the boundary temperature amplitudes gradually increase. This is because while an increase in temperature amplitude raises the temperature during half of the time and can accelerate the transport process, the temperature will also decrease in the other half and hinder the transport process. So, the two effects cancel each other, making the final concentration distribution less variable.

4.3. *Effect of period length of* $\boldsymbol{h_s(t)}$ *and* $\boldsymbol{T_s(t)}$ *on chloride transport*

Finally, this section remains the average and amplitude value of boundary conditions constant and compares chloride concentration profiles under different period lengths of boundary humidity and temperature. The detailed input parameters of $h_s(t)$ and $T_s(t)$ are listed in Table 7.

Fig. 14 shows the modelled total chloride concentration after 200 days. When the exposure time is the same, a longer period also implies a decrease in the number of cycles. So, it can be seen from the figures that the increase in period length has less effect on the final chloride distribution profiles. Combining Sections 4.1, 4.2 and 4.3, it can be concluded that the variation of humidity and temperature average can alter the peak values of chloride content but has less effect on the chloride penetration depth. However, the humidity amplitude change during cyclic wetting-drying processes could significantly affect both the peaks and the penetration depths, whereas other factors have less impact on the chloride transport process at a constant exposure time.

5. Conclusions

This study proposed a numerical model to investigate the chloride

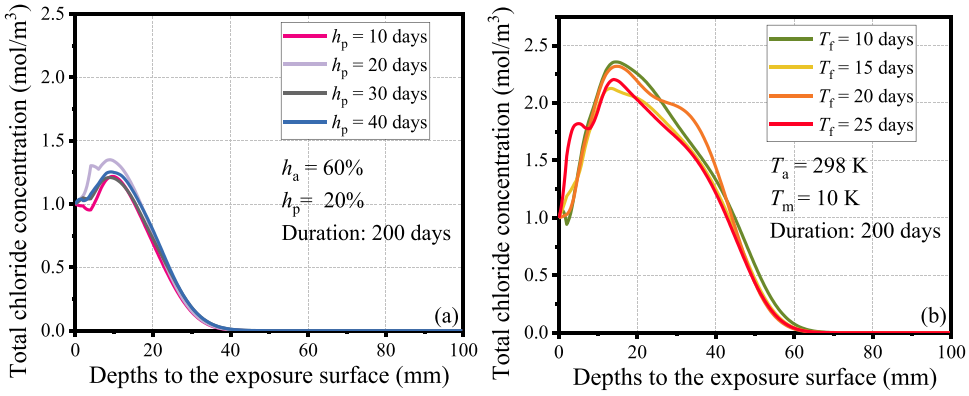

Fig. 14 Chloride concentration profiles at different period lengths of (a) $h_s(t)$ and (b) $T_s(t)$.

penetration in concrete under varying humidity and temperature changes. The interaction between moisture and heat transfer and their coupled effect on chloride transport are analysed. The predicted chloride distributions under different environments are compared with published experimental data. The following conclusions can be drawn:

(1) Considering the heterogeneous features of unsaturated concrete, the thermal conductivities of concretes with different volume fractions of aggregates, saturation degree and $m_{w/c}$ can be predicted through the proposed thermal conductivity model. The predicted results show that the thermal conductivity of concrete in a dry state will also increase with the increasing volume fraction of coarse aggregates and saturation degree. In contrast, it has a decreasing trend with the rising water to cement ratio.
(2) For the coupled moisture and heat transfer, the elevated temperature can promote moisture transport, and the increased water saturation will also accelerate the heat transfer. If the interaction between moisture and heat transfer is ignored, the predicted relative humidity and temperature will be underestimated.
(3) The chloride transport under varying humidity and temperature changes depends on the combined chloride diffusion and convection processes. The increased temperature will promote the chloride transport process. A non-linear relationship exists between temperature and the chloride binding capacity. Due to the cyclic W/D processes, the convection process will significantly accumulate chloride content near the exposure surface. The increasing wetting time will lead to higher peak values in the chloride contents. However, the penetration depth of chloride ions is generally constant regardless of different W/D conditions.
(4) The proposed model can analyse the effect of average value, amplitude value and period length of cyclic environmental changes on the chloride transport process by assuming boundary conditions of moisture and heat transfer as trigonometric functions. The results indicate that variation in humidity and temperature averages can alter the peak values of chloride content but have less effect on the chloride penetration depth. However, the increased humidity amplitude could significantly promote both the peak values and the penetration depths, whereas other factors have less impact on the chloride transport process at a constant exposure time.

The present study introduces a one-dimensional numerical model for chloride penetration in OPC concrete under varying humidity and temperature conditions. However, several areas require further investigation. First, the model should be expanded from one-dimensional to two-dimensional or even three-dimensional to better represent real-world scenarios. Additionally, future work should further incorporate the coupling of moisture and heat transfer by considering the heat released and absorbed during the condensation and evaporation of moisture.

CRediT authorship contribution statement

Mingzhong Zhang: Writing – review & editing, Supervision, Methodology. **Branko Šavija:** Writing – review & editing, Supervision, Funding acquisition, Conceptualization. **Liang-yu Tong:** Writing – original draft, Visualization, Validation, Software, Methodology, Investigation, Data curation. **Qing-feng Liu:** Writing – review & editing, Supervision, Project administration, Methodology, Funding acquisition, Conceptualization. **Qing Xiang Xiong:** Writing – review & editing, Validation, Supervision, Conceptualization.

Declaration of Competing Interest

The authors declare that they have no known competing financial interests or personal relationships that could have appeared to influence the work reported in this paper.

Data availability

The data that has been used is confidential.

Acknowledgements

This work was funded by the National Key R&D Program of China (2024YFB3715100), the National Natural Science Foundation of China (52222805), and the Open Foundation of the State Key Laboratory of Subtropical Building and Urban Science (2023KA03).

Appendix

Table A
Parameters used in the proposed model

Parameters		Values or expressions	References
Coupled moisture and hear transfer			
D_d^{ref}	Moisture reference diffusion coefficient during drying process	$8.31 \times 10^{-10} m^2/s$	[15]
D_w^{ref}	Moisture reference diffusion coefficient during wetting process	$4.05 \times 10^{-11} m^2/s$	[15]
D_d^0	Moisture diffusion coefficient of concrete at dry state	$D_d^{ref}\frac{3(1-\nu_a)^2}{3-\nu_a}$	[69]
D_w^0	Moisture diffusion coefficient of concrete at saturated state	$D_w^{ref}\frac{3(1-\nu_a)^2}{3-\nu_a}$	[69]
h_c	Relative humidity when $D_h = D_d^0/2$	0.8	[49]
α	Ratio of minimum D_h to D_d^0	0.025	
n_1	Regression coefficient	6	
n_2	Regression coefficient	6	
U	Activation energy of the diffusion process	35000 J/mol	[15]
R	Gas constant	$8.14\ J \bullet mol^{-1} \bullet K^{-1}$	[32]
T_{ref}	Reference temperature	296 K	[82]
ρ	Density	Table 1 (including gas pores, liquid pores, aggregates and cement mortar)	[51,53, 56]
c	Specific hear capacity		
λ	Thermal conductivity		

(continued on next page)

Table A (*continued*)

Parameters		Values or expressions	References
v_a	Volume fraction of aggregates	Experimental mixtures	
$m_{w/c}$	Water to cement ratio	Experimental mixtures	
α_{HD}	Hydration degree of cement paste	$1-\exp(-3.15m_{w/c})$	[34]
ϕ_{cp}	Porosity of cement paste	$\frac{m_{w/c}-0.36\alpha_{HD}}{m_{w/c}+0.32}$	[55]
ϕ_c	Porosity of concrete	$\phi_{cp}(1-v_a)$	[51]
Chloride transport under varying humidity and temperature changes			
D_0	Chloride diffusivity in pore solution	2.03×10^{-9}	[83]
D_{cp}	Chloride diffusivity of saturated cement paste	$\frac{2\phi_{cp}^{2.75}D_0}{\phi_{cp}^{1.75}\left(1-\phi_{cp}\right)+14.44\left(1-\phi_{cp}\right)^{2.75}}$	[68]
D_c	Chloride diffusivity of saturated concrete considering the presence of aggregates	$D_{cp}\frac{3(1-v_a)^2}{3-v_a}$	[69]
r	Impact index of water saturation	1	[15]
A	Chloride binding parameters fitted based on experimental data	$0.00002T_C^2+0.0006T_C+0.0775$	[37,76]
B		$0.0001T_C^2-0.0031T_C+0.3995$	

References

[1] H.-L. Wang, J.-G. Dai, X.-Y. Sun, X.-L. Zhang, Characteristics of concrete cracks and their influence on chloride penetration, Constr. Build. Mater. 107 (2016) 216–225.
[2] Z. Meng, Q.-F. Liu, J. Xia, Y. Cai, X. Zhu, Y. Zhou, L. Pel, Mechanical–transport–chemical modeling of electrochemical repair methods for corrosion-induced cracking in marine concrete, Comput. -Aided Civ. Infrastruct. Eng. 37 (14) (2022) 1854–1874.
[3] C. Tongning, Z. Lijuan, S. Guowen, W. Caihui, Z. Ying, W. Pengshuo, X. Aoxue, Simulation of chloride ion transport in concrete under the coupled effects of a bending load and drying–wetting cycles, Constr. Build. Mater. 241 (2020) 118045.
[4] Z. Yu, Y. Chen, P. Liu, W. Wang, Accelerated simulation of chloride ingress into concrete under drying–wetting alternation condition chloride environment, Constr. Build. Mater. 93 (2015) 205–213.
[5] Q.-F. Liu, Progress and research challenges in concrete durability: ionic transport, electrochemical rehabilitation and service life prediction, RILEM Tech. Lett. 7 (2022) 98–111.
[6] L. Homan, A.N. Ababneh, Y. Xi, The effect of moisture transport on chloride penetration in concrete, Constr. Build. Mater. 125 (2016) 1189–1195.
[7] E.P. Nielsen, M.R. Geiker, Chloride diffusion in partially saturated cementitious material, Cem. Concr. Res. 33 (1) (2003) 133–138.
[8] T. Ishida, K. Maekawa, T. Kishi, Enhanced modeling of moisture equilibrium and transport in cementitious materials under arbitrary temperature and relative humidity history, Cem. Concr. Res. 37 (4) (2007) 565–578.
[9] H. Zheng, J.-G. Dai, W. Li, C.S. Poon, Influence of chloride ion on depassivation of passive film on galvanized steel bars in concrete pore solution, Constr. Build. Mater. 166 (2018) 572–580.
[10] Q.X. Xiong, L.-Y. Tong, Z. Zhang, C. Shi, Q.-F. Liu, A new analytical method to predict permeability properties of cementitious mortars: the impacts of pore structure evolutions and relative humidity variations, Cem. Concr. Compos. 137 (2023) 104912.
[11] G. Sun, Y. Zhang, W. Sun, Z. Liu, C. Wang, Multi-scale prediction of the effective chloride diffusion coefficient of concrete, Constr. Build. Mater. 25 (10) (2011) 3820–3831.
[12] L. Tong, J. Zhao, Z. Cheng, Chloride ion binding effect and corrosion resistance of geopolymer materials prepared with seawater and coral sand, Constr. Build. Mater. 309 (2021) 125126.
[13] N. Olsson, V. Baroghel-Bouny, L.-O. Nilsson, M. Thiery, Non-saturated ion diffusion in concrete – a new approach to evaluate conductivity measurements, Cem. Concr. Compos. 40 (2013) 40–47.
[14] L.F. Yang, R. Cai, B. Yu, Investigation of computational model for surface chloride concentration of concrete in marine atmosphere zone, Ocean Eng. 138 (2017) 105–111.
[15] D. Chen, K. Yang, D. Hu, J. Shi, A meso-stochastic research on the chloride transport in unsaturated concrete, Constr. Build. Mater. 273 (2021) 121986.
[16] Y. Zhang, Z. Yang, G. Ye, Dependence of unsaturated chloride diffusion on the pore structure in cementitious materials, Cem. Concr. Res. 127 (2020) 105919.
[17] Y. Zhang, M. Zhang, Transport properties in unsaturated cement-based materials–a review, Constr. Build. Mater. 72 (2014) 367–379.
[18] J.-H. Zhu, C. Zeng, M.-N. Su, Z.-W. Zeng, A. Zhu, Effectiveness of a dual-functional intervention method on the durability of reinforced concrete beams in marine environment, Constr. Build. Mater. 222 (2019) 633–642.
[19] K. Li, C. Li, Z. Chen, Influential depth of moisture transport in concrete subject to drying–wetting cycles, Cem. Concr. Compos. 31 (10) (2009) 693–698.
[20] Z. Zhang, M. Thiery, V. Baroghel-Bouny, Numerical modelling of moisture transfers with hysteresis within cementitious materials: verification and investigation of the effects of repeated wetting–drying boundary conditions, Cem. Concr. Res. 68 (2015) 10–23.
[21] W. Li, L. Guo, Peridynamic investigation of chloride diffusion in concrete under typical environmental factors, Ocean Eng. 239 (2021) 109770.
[22] S. Lian, T. Meng, Y. Zhao, Z. Liu, X. Zhou, S. Ruan, Experimental and theoretical analyses of chloride transport in recycled concrete subjected to a cyclic drying-wetting environment, Structures 52 (2023) 1020–1034.
[23] Y. Bai, Y. Wang, Y. Xi, Modeling the effect of temperature gradient on moisture and ionic transport in concrete, Cem. Concr. Compos. 106 (2020) 103454.
[24] Z. Jiang, Y. Xi, X. Gu, Q. Huang, W. Zhang, Modelling of water vapour sorption hysteresis of cement-based materials based on pore size distribution, Cem. Concr. Res. 115 (2019) 8–19.
[25] M. Isteita, Y. Xi, The effect of temperature variation on chloride penetration in concrete, Constr. Build. Mater. 156 (2017) 73–82.
[26] H. Zhao, K. Jiang, R. Yang, Y. Tang, J. Liu, Experimental and theoretical analysis on coupled effect of hydration, temperature and humidity in early-age cement-based materials, Int. J. Heat. Mass Transf. 146 (2020) 118784.
[27] S. Care, Effect of temperature on porosity and on chloride diffusion in cement pastes, Constr. Build. Mater. 22 (7) (2008) 1560–1573.
[28] T. Nguyen, S. Lorente, M. Carcasses, Effect of the environment temperature on the chloride diffusion through CEM-I and CEM-V mortars: an experimental study, Constr. Build. Mater. 23 (2) (2009) 795–803.
[29] L. Tong, Q. Liu, Modelling of concrete transport property by considering multi-scale heterogeneous characteristics, J. Build. Mater. 26 (10) (2023) 1062–1071.
[30] L. Tong, Q. Liu, Prediction model for diffusivity of unsaturated concrete by considering time-varying pore structure, J. Chin. Ceram. Soc. 51 (8) (2023) 1950–1961.
[31] Q.X. Xiong, L.-Y. Tong, J.K. Huang, J. Yang, Q.F. Liu, Salt crystallization in porous materials: a quasi-local transport model for evaluating pore filling process, Construct. Build. Mater. (2025).
[32] Q.-F. Liu, G.-L. Feng, J. Yang, L.-Y. Li, Ionic transport features in concrete composites containing various shaped aggregates: a numerical study, Compos. Struct. 183 (2018) 371–380.
[33] S. Yang, N. Ukrainczyk, A. Caggiano, E. Koenders, Numerical phase-field model validation for dissolution of minerals, Appl. Sci. (Switz). 11 (6) (2021) 2461.
[34] W.-Q. Jiang, X.-H. Shen, S. Hong, Z.-Y. Wu, Q.-F Liu, Binding capacity and diffusivity of concrete subjected to freeze-thaw and chloride attack: a numerical study, Ocean Eng. 186 (2019) 106093.
[35] L.-X. Mao, L.-Y. Li, Y. Wang, Q.F. Liu, Physicochemical modelling in chlorides migration in concrete with account of multi-species coupling, reaction kinetic and pore evolution, Constr. Build. Mater. (2025).
[36] M. Fenaux, E. Reyes, J.C. Gálvez, A. Moragues, Modelling the transport of chloride and other ions in cement-based materials, Cem. Concr. Compos. 97 (2019) 33–42.
[37] D.K. Panesar, S.E. Chidiac, Effect of cold temperature on the chloride-binding capacity of cement, J. Cold Reg. Eng. 25 (4) (2011) 133–144.
[38] L. Ecay, D. Grégoire, G. Pijaudier-Cabot, On the prediction of permeability and relative permeability from pore size distributions, Cem. Concr. Res. 133 (2020) 106074.
[39] T. Gimmi, S.V. Churakov, Water retention and diffusion in unsaturated clays: connecting atomistic and pore scale simulations, Appl. Clay Sci. 175 (2019) 169–183.
[40] L.-Y. Li, A pore size distribution-based chloride transport model in concrete, Mag. Concr. Res. 66 (18) (2014) 937–947.
[41] F. Ren, X. Chen, Q. Zeng, C. Zhou, Effects of pure carbonation on pore structure and water permeability of white cement mortars, Cement 9 (2022) 100040.
[42] S.-T. Kang, J.-S. Kim, Y. Lee, Y.-D. Park, J.-K. Kim, Moisture diffusivity of early age concrete considering temperature and porosity, KSCE J. Civ. Eng. 16 (1) (2011) 179–188.
[43] L.-Y Tong, Q.X. Xiong, Z. Zhang, X. Chen, G. Ye, Q.-F. Liu, A novel lattice model to predict chloride diffusion coefficient of unsaturated cementitious materials based on multi-typed pore structure characteristics, Cem. Concr. Res. 176 (2024) 107351.
[44] B. Cho, D. Park, J. Kim, H. Hamasaki, Study on the heat-moisture transfer in concrete under real environment, Constr. Build. Mater. 132 (2017) 124–129.

[45] S.D. Bahador, J.H. Cahyadi, Modelling of carbonation of PC and blended cement concrete, IES J. Part A: Civ. Struct. Eng. 2 (1) (2009) 59–67.
[46] P. Liu, Z. Yu, Y. Chen, Carbonation depth model and carbonated acceleration rate of concrete under different environment, Cem. Concr. Compos. 114 (2020) 103736.
[47] L.-Y. Tong, Q.-F. Liu, X. Xu, Q.X. Xiong, D.C.W. Tsang, Effect of carbonation on transport properties of cementitious materials under different environmental conditions: A pore-scale modelling, J. Clean. Prod. (2025).
[48] J. Li, F. Xie, G. Zhao, L. Li, Experimental and numerical investigation of cast-in-situ concrete under external sulfate attack and drying-wetting cycles, Constr. Build. Mater. 249 (2020) 118789.
[49] A.V. Saetta, B.A. Schrefler, R.V. Vitaliani, The carbonation of concrete and the mechanism of moisture, heat and carbon dioxide flow through porous materials, Cem. Concr. Res. 23 (4) (1993) 761–772.
[50] X. Chen, T. Sanchez, D. Conciatori, H. Chaouki, L. Sorelli, B. Selma, M. Chekired, Numerical modeling of 2D hygro-thermal transport in unsaturated concrete with capillary suction, J. Build. Eng. 45 (2022) 103640.
[51] S. Zhang, H. Zhou, H. Wang, Thermal conductive properties of solid-liquid-gas three-phase unsaturated concrete, Constr. Build. Mater. 232 (2020) 117242.
[52] E. Samson, J. Marchand, Modeling the effect of temperature on ionic transport in cementitious materials, Cem. Concr. Res. 37 (3) (2007) 455–468.
[53] K.-H. Kim, S.-E. Jeon, J.-K. Kim, S. Yang, An experimental study on thermal conductivity of concrete, Cem. Concr. Res. 33 (3) (2003) 363–371.
[54] L.-Y. Tong, Q.-F. Liu, Q. Xiong, Z. Meng, Q. Amiri, M. Zhang, Modelling the chloride transport in concrete from microstructure generation to chloride diffusivity prediction, Comput. Aided Civ. Infrastruct. Eng. (2025), https://doi.org/10.1111/mice.13331.
[55] L.-Y. Tong, Q.X. Xiong, M. Zhang, Z. Meng, F. Meftah, Q.-F. Liu, Multi-scale modelling and statistical analysis of heterogeneous characteristics effect on chloride transport properties in concrete, Constr. Build. Mater. 367 (2023) 130096.
[56] W. Zhang, H. Min, X. Gu, Y. Xi, Y. Xing, Mesoscale model for thermal conductivity of concrete, Constr. Build. Mater. 98 (2015) 8–16.
[57] K. Boomsma, D. Poulikakos, On the effective thermal conductivity of a three-dimensionally structured fluid-saturated metal foam, Int. J. Heat. Mass Transf. 44 (4) (2001) 827–836.
[58] X. Gao, Z. Peng, L.-Y. Tong, Y. Cai, J. Xiao, X. Geng, Q.-F. Liu, Effect of global aggregate distribution on interfacial transition zones in cement-based materials: An analytical-numerical study, Constr. Build. Mater. 458 (2025) 138278.
[59] X. Gao, Q.-F. Liu, Y. Cai, L.-Y. Tong, Z. Peng, Q.X. Xiong, G.D. Schutter, A new model for investigating the formation of interfacial transition zone in cement-based materials, Cem. Concr. Res. 187 (2025) 107675.
[60] D.P.H. Hasselman, L.F. Johnson, Effective thermal conductivity of composites with interfacial thermal barrier resistance, J. Compos. Mater. 21 (6) (1987) 508–515.
[61] Q.-F. Liu, D. Easterbrook, J. Yang, L.-Y. Li, A three-phase, multi-component ionic transport model for simulation of chloride penetration in concrete, Eng. Struct. 86 (2015) 122–133.
[62] L.-Y. Tong, Y. Cai, Q.-F. Liu, Carbonation modelling of hardened cementitious materials considering pore structure characteristics: A review, J. Build. Eng. 96 (2024) 110547.
[63] T.Q. Nguyen, J. Petković, P. Dangla, V. Baroghel-Bouny, Modelling of coupled ion and moisture transport in porous building materials, Constr. Build. Mater. 22 (11) (2008) 2185–2195.
[64] W. Chen, Q. Liu, Moisture and multi-ions transport in concrete under drying-wetting cycles: a numerical study, J. Hydraul. Eng. 52 (5) (2021) 622–632.
[65] Z. Meng, Y. Zhang, W.-K. Chen, et al., A numerical study of moisture and ionic transport in unsaturated concrete by considering multi-ions coupling effect, Transp. Porous Media 151 (2) (2024) 339–366.
[66] M. Nizovtsev, S. Stankus, A. Sterlyagov, V. Terekhov, R. Khairulin, Determination of moisture diffusivity in porous materials using gamma-method, Int. J. Heat. Mass Transf. 51 (17-18) (2008) 4161–4167.
[67] P. O'Neill Iqbal, T. Ishida, Modeling of chloride transport coupled with enhanced moisture conductivity in concrete exposed to marine environment, Cem. Concr. Res. 39 (4) (2009) 329–339.
[68] J. Zheng, Z. Xinzhu, Analytical solution for the chloride diffusivity of hardened cement paste, J. Mater. Civ. Eng. 20 (5) (2008) 384–391.
[69] S.E. Chidiac, M. Shafikhani, Phenomenological model for quantifying concrete chloride diffusion coefficient, Constr. Build. Mater. 224 (2019) 773–784.
[70] J. Xu, Y. Song, L. Jiang, W. Feng, Y. Cao, W. Ji, Influence of elevated temperature on release of bound chlorides from chloride-admixed plain and blended cement pastes, Constr. Build. Mater. 104 (2016) 9–15.
[71] W.-Q. Jiang, X.-H. Shen, J. Xia, L.-X. Mao, J. Yang, Q.-F. Liu, A numerical study on chloride diffusion in freeze-thaw affected concrete, Constr. Build. Mater. 179 (2018) 553–565.
[72] Q.-F. Liu, Y. Cai, H. Peng, Z. Meng, S. Mundra, A. Castel, A numerical study on chloride transport in alkali-activated fly ash/slag concretes, Cem. Concr. Res. 166 (2023) 107094.
[73] N. Damrongwiriyanupap, L. Li, S. Limkatanyu, Y. Xi, Temperature effect on multi-ionic species diffusion in saturated concrete, Comput. Concr. 13 (2) (2014) 149–171.
[74] Y. Yu, X. Chen, W. Gao, D. Wu, A. Castel, Modelling non-isothermal chloride ingress in unsaturated cement-based materials, Constr. Build. Mater. 217 (2019) 441–455.
[75] J. Li, W. Shao, The effect of chloride binding on the predicted service life of RC pipe piles exposed to marine environments, Ocean Eng. 88 (2014) 55–62.
[76] A. Dousti, M. Shekarchi, Effect of exposure temperature on chloride-binding capacity of cementing materials, Mag. Concr. Res. 67 (15) (2015) 821–832.
[77] ISO, Thermal insulation-Determination of steady-state thermal resistance and related properties-Heat flow meter apparatus, ISO (International Organization for Standardization), Geneva, Switzerland, 1991.
[78] S.E. Gustafsson, Transient plane source techniques for thermal conductivity and thermal diffusivity measurements of solid materials, Rev. Sci. Instrum. 62 (3) (1991) 797–804.
[79] Y. Wang, Y. Xi, The effect of temperature on moisture transport in concrete, Mater. (Basel) (8) (2017) **10**.
[80] C. Sun, L. Yuan, X. Zhai, F. Qu, Y. Li, B. Hou, Numerical and experimental study of moisture and chloride transport in unsaturated concrete, Constr. Build. Mater. 189 (2018) 1067–1075.
[81] C. Chen, L. Wang, R. Liu, P. Zhu, H. Liu, X. Wang, J. Yu, Y. Chen, Chloride penetration of concrete exposed to dry-wet cycle with various dry-wet ratios and temperature, Constr. Build. Mater. 400 (2023) 132883.
[82] X. Zhu, G. Zi, Z. Cao, X. Cheng, Combined effect of carbonation and chloride ingress in concrete, Constr. Build. Mater. 110 (2016) 369–380.
[83] M. Achour, F. Bignonnet, J.-F. Barthélémy, E. Rozière, O. Amiri, Multi-scale modeling of the chloride diffusivity and the elasticity of Portland cement paste, Constr. Build. Mater. 234 (2020) 117124.